

Abstract

Clouds play an important role in balancing the Earth's radiation budget. Clouds reflect sunlight which cools the Earth, and also trap infrared radiation in the same manner as greenhouse gases. Changes in cloud cover and cloud properties over time can have important consequences for climate. The Intergovernmental Panel for Climate Change (IPCC) has identified current gaps in the understanding of clouds and related climate feedback processes as a leading cause of uncertainty in forecasting climate change. In this paper we present an algorithm that uses optimal estimation to retrieve cloud parameters from satellite multi-spectral imager data, in particular the Along-Track Scanning Radiometers ATSR-2 and AATSR. The cloud parameters retrieved are the cloud top pressure, cloud optical depth, cloud effective radius, cloud fraction and cloud phase. Importantly, the technique also provides estimated errors along with the retrieved values and quantifies the consistency between retrieval representation of cloud and satellite radiances. This should enable the effective use of the products for comparison with climate models or for exploitation via data assimilation. The technique is evaluated by performing retrieval simulations for a variety of simulated single layer and multi-layer conditions. Examples of applying the algorithm to ATSR-2 flight data are presented and the sensitivity of the retrievals assessed. This algorithm has been applied to both ATSR-2 and AATSR visible and infrared measurements in the context of the GRAPE (Global Retrieval and cloud Product Evaluation) project to produce a 14 year consistent record for climate research (Sayer et al., 2010).

1 Introduction

Clouds have long been recognised as one of the key moderators of the Earth's atmosphere: low clouds such as stratus effectively reflect incoming solar radiation, giving an overall cooling effect, while high clouds may partially transmit solar radiation but

AMTD

4, 2389–2431, 2011

Cloud retrieval algorithm

C. A. Poulsen et al.

Title Page

Abstract

Introduction

Conclusions

References

Tables

Figures

◀

▶

◀

▶

Back

Close

Full Screen / Esc

Printer-friendly Version

Interactive Discussion



effectively trap the outgoing thermal radiation, resulting in an overall warming effect. The balance between these effects and in particular how it might change over time, involving processes such as water vapour-feedback and cloud-aerosol interaction, significantly complicates prediction of future climate, as has been recognised by the Inter-
5 governmental Panel on Climate Change (IPCC).

In order to test climate models we require accurate, consistent, long-term, well characterised, global measurements of clouds and their properties. Ground-based observations are important, but these observations are often biased towards land and populated centres. Only satellites provide truly global coverage, which is essential for comparison with climate models. Various active and passive satellite cloud climatologies exist; for example, the active Cloud Profiling Radar (CPR) (Stephens et al., 2008) and Cloud-Aerosol Lidar with Orthogonal Polarization (CALIOP) sensors are able to provide height-resolved information on cloud properties (Winker et al., 2007), however coverage is limited to the sub-satellite track and the time-series are short. Of the passive
10 satellite instruments the most widely known are the High resolution Infrared Sounder (HIRS, Wylie et al., 1999), Moderate Resolution Imaging Spectroradiometer (MODIS, Platnick et al., 2003), Advanced Very High Resolution Radiometer (AVHRR, Jacobowitz et al., 2003; Heidinger et al., 2009) and Multi-angle imaging SpectroRadiometer (MISR, Moroney et al., 2002) data sets. The passive sensors cannot represent the complex
15 vertical structure but have much better global coverage and longer time series than active instruments. Typically information on optical depth is derived from the visible and near infrared channels (Nakajima et al., 1990) while information on the cloud top pressure is derived separately from infrared measurements using brightness temperatures, the split window technique or through CO₂ slicing algorithms. MISR lacks thermal infrared channels and instead uses stereoscopic observations from its multiple viewing
20 directions to derive cloud top height. This technique is also used to derive cloud top heights from Along Track Scanning Radiometer (ATSR) measurements (Muller et al., 2007). The International Satellite Cloud Climatology Project (ISCCP, Rossow et al., 1991) comprises a merging of polar and geostationary satellite data which has been
25

**Cloud retrieval
algorithm**

C. A. Poulsen et al.

[Title Page](#)[Abstract](#)[Introduction](#)[Conclusions](#)[References](#)[Tables](#)[Figures](#)[◀](#)[▶](#)[◀](#)[▶](#)[Back](#)[Close](#)[Full Screen / Esc](#)[Printer-friendly Version](#)[Interactive Discussion](#)

a fundamental, reference data-set of global cloud properties for many years, though shortcomings of this dataset have been identified (Evan et al., 2007).

Progress in understanding the global distribution of cloud and its evolution with time are expected to come from systematic inter-comparison of results from different sensors or from different retrieval approaches (e.g. via activities of Global Energy and Water cycle EXperiment, GEWEX), as well as model/measurement intercomparisons (e.g. CFMIP, Bodas et al., 2008). Here we describe an optimal estimation (OE) (Rodgers, 2000) approach to generate a data-set from the Along-Track Scanning Radiometers (ATSR-2 and AATSR) which should provide a valuable contribution in this area. Advantages of the dataset stem from both the retrieval method and from the characteristics of the ATSR observations:

- The ATSRs provide a long time-series (from 1995–present) of consistent, well-calibrated observations in 6 channels sensitive to cloud properties, spanning the visible to infrared spectral range, obtained in two viewing directions along-track. This time-series will continue into the foreseeable future via SLSTR on Sentinel-3.
- The OE scheme is based on fitting a physically consistent model of cloud to observations spanning the visible to mid-infrared, extracting information on the height, optical depth, particle size and phase of cloud, while rigorously treating model and observation errors. This in turn provides detailed estimation of the errors in the retrieved quantities, and quantification of the “goodness of fit” of the observations to the cloud forward model. This enables, the appropriateness of underlying assumptions in the retrieval to be tested and data interpreted accordingly. Furthermore, where the retrieval obtains a good fit to observed radiances, one can be assured that the resulting cloud properties provide simultaneously a good representation of the short wave and long wave radiative effects of the observed cloud, Ham et al. (2009) and Siddans et al. (2009) show large discrepancies between observed MODIS radiances and those predicted based on MODIS cloud retrievals. Such discrepancies are inherently avoided by the retrieval method adopted here.

Cloud retrieval algorithm

C. A. Poulsen et al.

Title Page

Abstract

Introduction

Conclusions

References

Tables

Figures

◀

▶

◀

▶

Back

Close

Full Screen / Esc

Printer-friendly Version

Interactive Discussion



In this paper we describe the optimal estimation algorithm, the sensitivity to the retrieved parameters for a range of cloud conditions including multi-layer cloud, and finally show some examples of the retrieval algorithm as it has been applied to ATSR-2 data.

This algorithm has been applied to the ATSR-2 and AATSR record from 1995–2009. The retrievals have already been used to analyse ship tracks (Campmany et al., 2009, Sayer et al., 2010) and study cloud-aerosol interactions (Bulgin et al., 2008). It is noted that, while the authors have applied the algorithm to the ATSR instrument, the method could in fact be applied to many different passive visible and infrared remote sensing instruments. Indeed, the theoretical basis for the algorithm was established through a Eumetsat study to derive cloud properties for the Meteosat Second Generation SEVIRI instrument (Watts et al., 1998). A version of the algorithm for SEVIRI is under development at Eumetsat.

An analogous technique for retrieving aerosol properties has been described in Thomas et al. (2009b).

2 The Along Track Scanning Radiometer (ATSR)

The ATSRs are dual-viewing imaging instruments measuring visible and infrared radiances (at 0.55, 0.67, 0.87, 1.6, 3.7, 11 and 12 μm) with 1 km spatial resolution at the sub-satellite point. ATSR-2 (Mutlow et al., 1999) was successfully launched on-board the ESA satellite ERS-2 on the 21 April 1995 and data were routinely produced from June 1995 to October 2008. A similar instrument AATSR (Advanced ATSR, Llewellyn-Jones et al., 2001) was launched on board Envisat in March 2002 and is still currently operational. AATSR is scheduled to be followed by a new instrument based on ATSR design principles called the Sea and Land Surface Temperature Radiometer (SLSTR) on board Sentinel-3, which is scheduled for launch in 2013. ATSR-1 (which lacks the visible channels) operated on ERS-1 from 1992–2000.

Cloud retrieval algorithm

C. A. Poulsen et al.

Title Page

Abstract

Introduction

Conclusions

References

Tables

Figures

◀

▶

◀

▶

Back

Close

Full Screen / Esc

Printer-friendly Version

Interactive Discussion



Cloud retrieval algorithm

C. A. Poulsen et al.

[Title Page](#)[Abstract](#)[Introduction](#)[Conclusions](#)[References](#)[Tables](#)[Figures](#)[◀](#)[▶](#)[◀](#)[▶](#)[Back](#)[Close](#)[Full Screen / Esc](#)[Printer-friendly Version](#)[Interactive Discussion](#)

The ATSRs are designed to have exceptional long term sensitivity and stability of calibration. Thermal channels are calibrated using two on-board black bodies at known temperatures which are observed during each across-track scan of the instrument. This makes it possible to determine single channel equivalent brightness temperatures correct to ± 0.05 K (Smith et al., 2001). The instrument also has an on-board visible/rear-ir calibration system enabling the visible channels to be calibrated to an accuracy of better than 4% (Smith et al., 2008), which is subsequently improved via vicarious calibration using scenes of known stable surface BRDF (certain deserts and ice caps). The specifications of the different ATSR instruments can be found in Table 1.

The excellent calibration and long time series of the ATSR instruments, as well as substantial overlap periods to enable inter-instrument calibration, make ATSR measurements well suited to generate record suitable for climate science.

3 Cloud retrieval scheme

The ATSR instruments' primary scientific mission is to perform high-accuracy sea surface retrievals (Mutlow et al., 1994), which requires accurate detection of cloud-affected scenes. The instruments are also suitable for the retrieval of cloud-properties, since the 7 channels are sensitive in different ways to the macro and microphysical properties of cloud. For example the infrared channels provide useful extra information to the visible channels in the case of optically thin clouds. However the observations are certainly not sensitive to every aspect of the three-dimensional distribution of all relevant cloud properties and no single channel is uniquely sensitive to a specific cloud property. We approach the problem of extracting useful information on cloud as an inverse problem: A forward model (FM) is defined which applies a radiative transfer model (RTM) to simulate satellite radiances based on a parametrised cloud/atmosphere/surface model (CM) and the defined observing conditions. An inverse or retrieval model (RM) is then used to obtain the cloud parameters which give the best fit between the model predicted and observed radiances, taking into account measurement errors and relevant

prior knowledge. This inverse problem is solved using the optimal estimation method (Rodgers, 2000) (OEM):

The basic principle of the OEM is to maximise the probability of the retrieved state, conditional on the value of the measurements and any a priori knowledge. Formally, it is required to maximise the conditional probability $P = P(x|y, x_a)$ with respect to the values of the measurement vector \mathbf{y} and state vector \mathbf{x} . x_a is the a priori estimate of the state, i.e. the most likely state prior to taking the measurements into account. The assumption is made that errors in the measurements (and forward model) and a priori parameters are normally distributed with zero mean and covariances given by \mathbf{S}_y and \mathbf{S}_a , respectively. The solution state is found by minimising the cost function, J ;

$$J(\mathbf{x}) = (\mathbf{y}(\mathbf{x}) - \mathbf{y}_m) \mathbf{S}_y^{-1} (\mathbf{y}(\mathbf{x}) - \mathbf{y}_m)^T + (\mathbf{x} - \mathbf{x}_a) \mathbf{S}_a^{-1} (\mathbf{x} - \mathbf{x}_a)^T \quad (1)$$

The cost function can be minimised by estimating its gradient (by linearising the forward model) for an initial estimate of the state. Using this gradient, an estimate of the state is made which is predicted to have lower cost. The procedure is iterated until convergence (or the attempt to reach convergence is abandoned). Here, the Levenberg-Marquart (Marquardt, 1963; Levenberg, 1944) scheme is used to perform the minimisation. Convergence is judged to occur when the cost function changes by less than 1 between iterations. Retrievals which do not converge after 25 iterations are considered invalid.

If the a priori and measurements errors are well represented by their respective covariances, then the cost function value at solution is expected to follow a χ^2 distribution with degrees of freedom equal to the total number of elements in the measurement and state vectors. The value of the cost function therefore provides a measure of the likelihood of the solution-state being consistent with observations and prior knowledge.

For retrievals which satisfactorily converge, i.e. converge to a minimum cost which is consistent with measurement and prior errors, then the errors on the estimated state parameters are described by the solution covariance:

$$\mathbf{S}_x = (\mathbf{K}^T \mathbf{S}_y^{-1} \mathbf{K} + \mathbf{S}_a^{-1})^{-1} \quad (2)$$

Cloud retrieval algorithm

C. A. Poulsen et al.

Title Page

Abstract

Introduction

Conclusions

References

Tables

Figures

◀

▶

◀

▶

Back

Close

Full Screen / Esc

Printer-friendly Version

Interactive Discussion



where \mathbf{K} contains the derivatives of the forward model with respect to each solution state parameter:

$$K_{ij} = \frac{\delta y_i}{\delta x_j} \quad (3)$$

4 Cloud/atmosphere/surface model

Here we assume each AATSR scene to be composed of a clear-sky fraction and a cloudy fraction. The clear-sky atmosphere is defined by temperature and humidity profiles taken from ECMWF analyses (ECMWF, 2008). A fixed mid-latitude ozone profile is assumed (relevant for modelling atmospheric transmission in the visible channels).

The surface is assumed to be a Lambertian reflector. Over sea the algorithm uses the model of Cox and Munk (1954a) and Cox and Munk (1954b) (using winds from ECMWF). Over land the MODIS albedo product for the year 2002 has been used in the processing of ATSR-2 and for AATSR. Error on the modelled surface albedo is addressed via the assumed measurement covariances (see Sect. 6, below). For the infrared channels the surface is assumed to have an emissivity of 1. The temperature of the surface is a retrieved parameter (see Sect. 7).

The FM simulates radiances for the whole scheme by linearly weighting simulated radiances the clear-sky and cloudy parts of the scene by cloud fraction, f (also a retrieved parameter). Cloud is assumed to be a single, plane-parallel, layer of either liquid or ice particles. The layer is assumed to be geometrically infinitely thin and is placed within the clear-sky atmosphere model. The cloud layer is parametrised in terms of the following retrieved quantities:

- The cloud phase, i.e. ice or liquid.
- The effective radius, r_{eff} of the cloud particle size distribution.

Cloud retrieval algorithm

C. A. Poulsen et al.

Title Page

Abstract

Introduction

Conclusions

References

Tables

Figures

◀

▶

◀

▶

Back

Close

Full Screen / Esc

Printer-friendly Version

Interactive Discussion



- The total (vertically integrated) optical depth, τ of the cloud at a fixed wavelength of $0.55 \mu\text{m}$.
- The cloud top pressure, p_c .

Size distributions for ice and liquid cloud are defined as a function of only r_{eff} and τ . r_{eff} defines the shape of the modelled size distribution and τ defines implicitly the total number of particles. For ice clouds, single scattering properties (extinction coefficient, single scattering albedo and phase function) are taken from Baran et al. (2004). These are based on a mixture of ray tracing and T-Matrix methods. Size distributions themselves are those of warm Uncinus cirrus cloud (Takano et al., 1989) with scaled distributions to give a range of effective radii. Single scattering properties of liquid cloud are derived by Mie theory assuming a modified gamma size distribution of particle radius r :

$$n(r) = 2.373 r^6 \exp\left(-\frac{6r}{r_m}\right) \quad (4)$$

where r_m is the mode radius of the distribution. The radiatively significant effective radius, r_{eff} , is given by

$$r_{\text{eff}} = \frac{\int_0^\infty r \pi r^3 n(r) dr}{\int_0^\infty \pi r^2 n(r) dr} \quad (5)$$

This approach reduces the complexity of cloud to a simple model with parameters which can be distinguished using the channels available on the ATSRs: the visible channel radiances are predominantly controlled by the cloud optical depth. Near-ir channels are also sensitive to particle size and phase due to the dependence on size of the single-scattering albedo in that spectral range, and the associated differences between ice and liquid phase particles. Thermal channels predominantly provide information on cloud-top pressure (via the dependence of the cloud thermal emission on

Cloud retrieval algorithm

C. A. Poulsen et al.

Title Page

Abstract

Introduction

Conclusions

References

Tables

Figures

◀

▶

◀

▶

Back

Close

Full Screen / Esc

Printer-friendly Version

Interactive Discussion



the atmospheric temperature profile). However it is acknowledges that no single channel or set of channels contributes to the retrieval of a cloud parameter. All channels are sensitive to a greater or lesser extent dependant on the scene.

We recognised that this simple model cannot represent all aspects of cloud three-dimensional structure. In the ideal case, the retrieved parameters should correspond to vertical (over the profile) and horizontal (over the scene) averages of the “true” cloudy properties. However there are classes of clouds, particularly those with strong vertical variations in particle size and phase, for which this model cannot predict radiances simultaneously consistent with observations in all ATSR channels. This condition can be recognised by checking that the retrieval converges with satisfactory cost.

In Sect. 10 we specifically test the performance of the scheme under varied multi-layer cloud conditions, diagnosing under what conditions the retrieval provides a good solution (within estimated errors of the true state) and whether the solution cost can effectively be used to distinguish conditions in which the model assumptions are inappropriate.

5 Radiative transfer model

Distinct RTMs are used for the solar (0.55, 0.67, 0.87 and 1.6 μm) and thermal (11 and 12 μm) channels. Fast radiative transfer is necessary to enable retrievals to be performed within practical computational constraints. To achieve the necessary speed both models have the following common aspects:

- The effects of multiple-scattering are accounted for using pre-computed look-up-tables LUTs. These tables contain the values of the following parameters $R_{\text{CLD}}(\tau, r_{\text{eff}}, \omega_0, \omega_r)$, $R_{\text{CLD}}(\tau, r_{\text{eff}}, 2\pi, 2\pi)$, $R_{\text{CLD}}(\tau, r_{\text{eff}}, 2\pi, \omega_r)$, $T_{\text{CLD}}(\tau, r_{\text{eff}}, 2\pi, \omega_r)$, $T_{\text{CLD}}(\tau, r_{\text{eff}}, \omega_0, 2\pi)$ and $\varepsilon_{\text{CLD}}(\tau, r_{\text{eff}})$, which are defined below. Values are stored at discrete values of τ , r_{eff} , ω_0 and ω_r (where appropriate). LUTs are pre-computed using DISTORT (Stamnes et al., 1988). During retrievals they are linearly interpolated to obtain the required values.

Cloud retrieval algorithm

C. A. Poulsen et al.

Title Page

Abstract

Introduction

Conclusions

References

Tables

Figures

◀

▶

◀

▶

Back

Close

Full Screen / Esc

Printer-friendly Version

Interactive Discussion



Cloud retrieval algorithm

C. A. Poulsen et al.

Title Page

Abstract

Introduction

Conclusions

References

Tables

Figures

◀

▶

◀

▶

Back

Close

Full Screen / Esc

Printer-friendly Version

Interactive Discussion



- Radiative transfer is performed in quasi-monotonically. I.e. a single radiative transfer calculation is performed for each channel, taking as input channel spectral-response function convolved optical properties (e.g. clear-sky transmission to cloud layer, cloud single-scattering properties).
- Derivatives with respect to state-vector elements (i.e. the elements of \mathbf{K}) are analytically computed.

Details of the solar and thermal RTMs are provided below.

5.1 Visible and near-ir RTM

Each ATSR short wave channel measures the radiance in the instrument's field-of-view, defined by the solid angle Δ_{FOV} . Each channel also has a relative spectral response $\varrho(\lambda)$ within a wavelength interval $[\lambda_1, \lambda_2]$ and has zero response outside this band. Under these conditions the radiance measured by the instrument is

$$L_{\bar{\lambda}}^r(\omega_r) = \frac{\int_0^{\Delta_{\text{FOV}}} \int_{\lambda_1}^{\lambda_2} L_{\lambda}^r(\lambda, \omega) \varrho(\lambda) d\lambda d\omega}{\int_0^{\Delta_{\text{FOV}}} d\omega}, \quad (6)$$

where ω is used to represent the spherical coordinate zenith and azimuth angle pair (θ, ϕ) and the integral over solid angle has been abbreviated as

$$\int_0^{\Delta\omega} d\omega = \int_0^{2\pi} \int_0^{\Delta\theta} \sin\theta d\theta d\phi. \quad (7)$$

The “Sun-normalised radiance” (or top of atmosphere reflectance) can then be formed by dividing the measured radiance $L_{\bar{\lambda}}^r(\omega_r)$ by $E_{\bar{\lambda}}^0$, the irradiance the satellite would measure if viewing the Sun through a perfect diffuser i.e.

$$R(\bar{\lambda}, \omega_0, \omega_r) = \frac{\pi L_{\bar{\lambda}}^r(\omega_r)}{\cos\theta_0 E_{\bar{\lambda}}^0}. \quad (8)$$

Cloud retrieval algorithm

C. A. Poulsen et al.

Title Page

Abstract

Introduction

Conclusions

References

Tables

Figures

◀

▶

◀

▶

Back

Close

Full Screen / Esc

Printer-friendly Version

Interactive Discussion



The factor $\cos \theta_0$ accounts for the reduction in energy per unit area when the Sun's energy strikes the atmosphere-Earth system at an angle θ_0 to the local vertical.

In the limit of a very narrow band, the measured Sun normalised radiance is a good approximation to the spectral bidirectional reflectance factor $R(\lambda, \omega_i, \omega_r)$ which is defined as the ratio of the reflected radiant flux to the reflected radiant flux from an ideal diffuse (i.e. Lambertian) surface (Schaepman-Strub et al., 2006). The bidirectional reflectance factor is a function of the wavelength λ and the input and output directions represented by ω_i and ω_r respectively. For simplicity, the dependence of reflection and transmittance on λ will not be explicitly shown.

For the cloudy fraction of a scene the atmosphere is modelled as having three layers: a below-cloud layer, a cloud layer and an above-cloud layer. The above and below-cloud layers consist of gaseous absorbers that attenuate radiation without scattering.

The gaseous absorption optical depth of the atmosphere is calculated by MODTRAN (Berk et al., 1989) using standard atmospheric profiles for different latitude bands. This total absorption optical depth is then partitioned into the above cloud optical depth τ_{ac} and the below cloud optical depth τ_{bc} based on the cloud top pressure relative to the surface pressure.

The surface is assumed Lambertian with reflectance R_{SFC} . This means that the directionality of the radiance onto the surface can be ignored. The advantage of this formulation is that the multiple scatters between the cloud and the surface are contained in irradiance terms. The multiple reflections between cloud and surface, shown stylistically in Fig. 1, give rise to a geometric series which can be evaluated analytically. The spectral bidirectional reflectance factor at the top of atmosphere is given by

$$\begin{aligned}
 R(\omega_0, \omega_r) = & e^{-\tau_{ac}/\cos \theta_0} [R_{CLD}(\omega_0, \omega_r) \\
 & + T_{CLD}(\omega_0, 2\pi) R_{SFC}(2\pi, 2\pi) T_{CLD}(2\pi, \omega_r) \\
 & + T_{CLD}(\omega_0, 2\pi) R_{SFC}(2\pi, 2\pi) R_{CLD}(2\pi, 2\pi) \\
 & \quad R_{SFC}(2\pi, 2\pi) T_{CLD}(2\pi, \omega_r) \\
 & + \dots] e^{-\tau_{ac}/\cos \theta_r}
 \end{aligned}$$

$$= e^{-\tau_{ac}/\cos \theta_0} \left[R_{\text{CLD}}(\omega_0, \omega_r) + \frac{T_{\text{CLD}}(\omega_0, 2\pi) R_{\text{SFC}}(2\pi, 2\pi) T_{\text{CLD}}(2\pi, \omega_r)}{1 - R_{\text{CLD}}(2\pi, 2\pi) R_{\text{SFC}}(2\pi, 2\pi)} \right] e^{-\tau_{ac}/\cos \theta_r} \quad (9)$$

where $T_{\text{CLD}}(\omega_0, 2\pi)$ is the cloud spectral directional-hemispherical total transmittance factor and $T_{\text{CLD}}(2\pi, \omega_0)$ is the cloud spectral hemispherical-directional total transmittance factor. The cloud spectral bihemispherical reflectance, $R_{\text{CLD}}(2\pi, 2\pi)$ or albedo can be calculated from the bidirectional reflectance factor using

$$R_{\text{CLD}}(2\pi, 2\pi) = \frac{1}{\pi} \int_0^{2\pi} \frac{1}{\pi} \int_0^{\pi/2} R_{\text{CLD}}(\omega_i, \omega_r) d\Omega_i d\Omega_r \quad (10)$$

To complete this model we parametrise the attenuation of the layer below the cloud

$$T_{bc}(2\pi, 2\pi) = e^{-\tau_{bc}/\cos 66^\circ} \quad (11)$$

where τ_{bc} is the optical thickness of the layer. This assumes the mean angle of below cloud transmittance is 66° . Including the below cloud absorption within the forward model gives

$$R_o(\omega_0, \omega_r) = e^{-\tau_{ac}/\cos \theta_0} \left[R_{\text{CLD}}(\omega_0, \omega_r) + \frac{T_{\text{CLD}}(\omega_0, 2\pi) R_{\text{SFC}}(2\pi, 2\pi) T_{\text{CLD}}(2\pi, \omega_r)}{1 - R_{\text{CLD}}(2\pi, 2\pi) R_{\text{SFC}}(2\pi, 2\pi) T_{bc}^2} \right] e^{-\tau_{ac}/\cos \theta_r} \quad (12)$$

The spectral bidirectional reflectance factor for the non-cloudy portion of the instruments view is given by the surface reflectance attenuated by the gaseous absorption of the atmospheric column, i.e.

$$R_o(\omega_0, \omega_r) = e^{-(\tau_{ac} + \tau_{bc})/\cos \theta_0} R_{\text{SFC}}(2\pi, 2\pi) e^{-(\tau_{ac} + \tau_{bc})/\cos \theta_r} \quad (13)$$

Cloud retrieval algorithm

C. A. Poulsen et al.

Title Page

Abstract

Introduction

Conclusions

References

Tables

Figures

◀

▶

◀

▶

Back

Close

Full Screen / Esc

Printer-friendly Version

Interactive Discussion



Hence the spectral bidirectional reflectance factor R of a pixel with fractional cloud cover f is given by

$$R = f R_{\bullet} + (1 - f) R_{\circ}. \quad (14)$$

5.2 Thermal-ir RTM

The thermal RTM makes extensive use of the RTTOV model (Saunders et al., 1999). RTTOV directly provides the modelled radiance from the clear-sky fraction of the scene.

The observed radiance for the cloudy part of the scene is modelled in terms of contributions from four terms: transmission of the radiance upwelling from below cloud level, emission from the cloud, reflection of radiance downwelling from above cloud level and emission of radiance from the atmosphere above the cloud.

$$L_{\bullet}^{\uparrow}(\omega_r) = \left(L_{bc}^{\uparrow}(\omega_r) T_{\text{CLD}}(2\pi, \omega_r) \right) + B \left(T_{\text{CLD}} \varepsilon_{\text{CLD}} + L_{ac}^{\downarrow} R_{\text{CLD}}(2\pi, \omega_r) \right) e^{-(\tau_{ac})} + L_{ac}^{\uparrow}(\omega_r) \quad (15)$$

RTTOV directly computes clear sky terms L_{bc}^{\uparrow} , the upward radiance at the cloud base, L_{ac}^{\downarrow} , the downward radiance at the cloud top from the atmosphere, and L_{ac}^{\uparrow} , the TOA radiance from the atmosphere above the cloud. ε_{CLD} is the cloud effective emissivity (computed by DISORT and tabulated in LUTs). $B(T_{\text{CLD}})$ is the Planck function for the temperature of the cloud (obtained by interpolation of the model temperature profile to ρ_c).

6 Measurement vector and covariance

The retrieval scheme described here uses nadir-view observations in the 0.55, 0.67, 1.6, 11 and 12 μm channels of the ATSRs. The 3.7 micron channels is not included because it has been found to be difficult to consistently represent both the 1.6 and

Cloud retrieval algorithm

C. A. Poulsen et al.

Title Page

Abstract

Introduction

Conclusions

References

Tables

Figures

◀

▶

◀

▶

Back

Close

Full Screen / Esc

Printer-friendly Version

Interactive Discussion



Cloud retrieval algorithm

C. A. Poulsen et al.

Title Page

Abstract

Introduction

Conclusions

References

Tables

Figures

◀

▶

◀

▶

Back

Close

Full Screen / Esc

Printer-friendly Version

Interactive Discussion



3.7 μm channels with the simple assumed CM (Baran et al., 2004). Similarly forward view radiances are not included as three-dimensional structure of cloud will often cause differences between the views which cannot be accommodated by the simple model. Note that the 0.55 μm channel is often not present due to the operating modes of the instrument. If present it is used. For computational efficiency the observations were processed for an average of 3 pixels across track and 4 pixels along track, this corresponds to approximately 3×3 km. The solution covariance used in the retrieval is the sum of four terms, see Eq. (16)

$$\mathbf{S}_y = \mathbf{S}_{\text{noise}} + \mathbf{S}_{\text{pixel}} + \mathbf{S}_{\text{fm}} \quad (16)$$

where $\mathbf{S}_{\text{noise}}$ represents random noise on the observations. The matrix is assumed diagonal with values on the diagonal equal to the square of the assumed measurement noise, namely .058, .009, .018 (all units of sun-normalised radiance), .21 K and .23 K respectively see Smith (2005) for the origin of these values.

$\mathbf{S}_{\text{pixel}}$ represents errors related to inadequacies of the plane parallel cloud model and imperfect co-registration of the channels. It is assumed diagonal with values equal to the square of 2.75%, 2.75% and 2.5% of the measured radiance in the visible and near-ir channels. For the two thermal channels (the square of) values of 0.1 K are assumed. See (Watts et al., 1998) for the derivation of this term.

\mathbf{S}_{fm} is 0 for rows and columns corresponding to the thermal channels. For the visible and near-ir channels, the matrix is intended to represent errors from the use of the MODIS surface albedo. Diagonal elements are set to (the square of) the albedo for the corresponding channel multiplied by 0.2. Off-diagonals are set to give a correlation between the visible/near-ir channels of 0.4.

7 State vector and a priori constraint

The state-vector used in the retrieval is as follows

- Log_{10} optical depth

- Cloud effective Radius
- Cloud top pressure
- Cloud fraction
- Surface temperature-measurements

5 A priori and first guess values depend on the assumed phase (phase determination is addressed in Sect. 8).

For liquid cloud, a priori values are 15, 8 μm , 800 hPa for optical depth, effective radius, cloud top pressure respectively, for ice the equivalent a priori values are 15, 30 μm , 400 hPa.

10 The surface temperature a priori value is taken from ECMWF model fields.

The a priori value for cloud-fraction (within the 3 \times 4 km analysed scene) is the fraction of full-spatial resolution pixels flagged as cloudy. Over sea the cloud flag used is that of Zavody et al. (2000). Over land the cloud flag used is that described in Birks (2004) which uses a NDVI (Normalised Difference Vegetation Index) technique. Retrievals are only performed for scenes with a non-zero cloud fraction.

15 The a priori error for each state parameter was set at 10^8 in the absence of useful information. This implies that the cloud optical depth effective radius and cloud top pressure are effectively unconstrained by their a priori value. For cloud fraction, the a priori error is set to 0.1 and for surface temperature it is 1 K over sea and 3 K over land.

20 The a priori covariance is assumed to be diagonal.

The initial (first-guess) values for state-vector parameters are set equal to the a priori values.

8 Phase determination

25 The only retrieved parameter not directly included in the state-vector is phase. Phase is retrieved as follows:

Cloud retrieval algorithm

C. A. Poulsen et al.

Title Page

Abstract

Introduction

Conclusions

References

Tables

Figures

◀

▶

◀

▶

Back

Close

Full Screen / Esc

Printer-friendly Version

Interactive Discussion



Cloud retrieval algorithm

C. A. Poulsen et al.

Title Page

Abstract

Introduction

Conclusions

References

Tables

Figures

◀

▶

◀

▶

Back

Close

Full Screen / Esc

Printer-friendly Version

Interactive Discussion



- At the beginning of a retrieval, the phase of the cloud is assumed to be ice or water based on the value of the calculated overcast brightness temperature of the 11 μm channel. The threshold between ice and water is assumed to be 260 K.
- The phase may be switched during the retrieval iteration according to the following criteria:
 - The phase change from liquid to ice is identified when the current estimate of r_{eff} exceeds 23 μm (provided the scheme has not converged to this value as its final solution). When this threshold is reached, the retrieval is restarted assuming the cloud to be ice.
 - Similarly if r_{eff} for ice cloud become lower than 20 μm the the retrieval is restarted assuming liquid. Only one change of phase is allowed in the retrieval.

It is recognised that ice clouds do exist with $r_{\text{eff}} < 20 \mu\text{m}$, and the retrieval will not provide reliable results in such situations. An alternative approach to the selection of cloud phase which would avoid this problem would be to simple run the retrieval twice, once for each phase, and select the most probable phase based on solution cost. However this is more computationally expensive and was therefore not implemented in large-scale processing runs to date.

9 Cloud ice and liquid path

In addition to the retrieved state parameters a number of cloud variables are derived and stored in the global level cloud products. Cloud water path, CWP, is derived using the method of Han et al. (1994)

$$\text{CWP} = \frac{4}{3} \times \frac{\tau \cdot r_{\text{eff}} \cdot \rho}{Q_{\text{ext}}} \quad (17)$$

where Q_{ext} , the extinction coefficient, is assumed to be 2 for water and 2.1 for ice, for wavelengths much less than r_{eff} . The density, ρ (g m^{-3}), is 1 for water and 0.91267 for

ice. Depending on phase, CWP is also known as liquid water path (LWP) or ice water path (IWP).

10 Retrieval scheme performance

In this section we examine the theoretical performance of the cloud retrieval algorithm in the configuration used when processing ATSR data for the GRAPE project. Three questions are addressed in terms of the retrievals sensitivity and our ability to identify situations when the retrieval does not perform well:

1. At what optical depths and effective radii does the retrieval algorithm perform well for single-layer clouds?
2. How well does the retrieval perform in the presence of multi-layer cloud, given the cloud model used is a single layer, and can we identify when a single cloud layer model is inappropriate?
3. How sensitive is the retrieval to assuming an incorrect cloud i.e. how well does the cloud retrieval perform when ice LUTS are applied to a liquid cloud and vice versa?

The questions are addressed by performing linear error simulations in the first case, and non-linear retrieval simulations for the last two questions.

10.1 Sensitivity study of single-layer cloud retrievals

In this section linear simulations are used to evaluate the sensitivity of observations to cloud parameters and error sources. The results are computed for a specific set of atmospheric profiles and observing conditions. Observation sensitivities are then transformed into retrieval sensitivity assuming that the cloud forward model is linear within some suitable range about the atmospheric/observing state.

Cloud retrieval algorithm

C. A. Poulsen et al.

Title Page

Abstract

Introduction

Conclusions

References

Tables

Figures

◀

▶

◀

▶

Back

Close

Full Screen / Esc

Printer-friendly Version

Interactive Discussion



Simulation setup

In addition to the retrieval setup outlined in Sect. 6, the linear simulations were performed for the following scenarios.

- Solar zenith angle 30° , relative azimuth 0° and satellite zenith angle 0° .
- The retrieval uses a standard temperature, humidity, and trace gas profile for northern mid-latitudes.
- The optical depths simulated were 0.01, 0.5, 1, 3, 5, 7, 10., 12, 15, 20, 25, 30, 50, 100 for liquid and ice clouds.
- The effective radii simulated were 3, 5, 6, 7, 8, 9, 10, 12, 14, 16, 18, 20, 22, 25 μm for liquid clouds, and 3, 5, 8, 10, 12, 15, 20, 25, 30, 35, 40, 50, 60 μm for ice clouds.
- The surface is assumed to be sea.
- Cloud fraction is fixed to 1.

Figure 2 shows the simulated retrieval errors, i.e. the square root of the error covariance, \mathbf{S}_x as a percentage of the expected retrieved parameter for a single layer of ice or liquid cloud with varying optical depth and effective radius. (Note that the radii range are different for the two different phases to reflect realistic scenarios.) The primary findings are

- The percentage uncertainty on the optical depth increases as clouds become optically thick and is high for very optically-thin clouds.
- The percentage uncertainty for the effective radius is highest for optically thin clouds and very small radii.
- The percentage uncertainty on the cloud top pressure is largest for very thin clouds.

Cloud retrieval algorithm

C. A. Poulsen et al.

Title Page

Abstract

Introduction

Conclusions

References

Tables

Figures

◀

▶

◀

▶

Back

Close

Full Screen / Esc

Printer-friendly Version

Interactive Discussion



- The percentage uncertainty for cloud liquid/ice path is greater for ice clouds and increases with optical depth and effective radius and is high for optically thin clouds.

From this simulation it is clear that with the current model, clouds optically thin, clouds with a small effective radii and extremely optically thick are difficult to retrieve with low retrieval error. This simulation assumes that the optical models of the liquid and ice cloud are correct, and uncertainty in the models would add uncertainty to the state. Ice clouds are more difficult to model than water clouds due to the variation in type i.e hexagonal aggregates, rosettes and the choice of optical model could have a significant effect on the accuracy of the retrieval (Zhang et al., 2009).

11 Simulations of multi-layer cloud

The frequent occurrence of multi-layer cloud is one of the most difficult problems facing passive satellite remote sensors of cloud (Chang et al., 2005). Incorrectly retrieving multi-layer cloud with a single layer cloud model could potentially result in incorrect and biased retrievals of the cloud properties. One of the most common types of multi-layer cloud is thin cirrus over stratus cloud and it is this situation that is investigated here. To evaluate the effect of this category of multi-layer clouds we apply the cloud retrieval scheme to a set of simulated radiances. The radiances are generated by assuming varying optical thickness for each layer. The simulations are performed separately assuming liquid and ice optical properties. The effect of using ice cloud optical properties when retrieving a liquid cloud, and vice-versa, is also discussed.

Simulation setup

The simulation was setup as in Sect. 10.1 with the following extra conditions

- The “true” values of the simulated cloud are 320 hPa and 780 hPa cloud top pressure and 50 μm and 12 μm effective radius for the ice and liquid cloud respectively.

Cloud retrieval algorithm

C. A. Poulsen et al.

Title Page

Abstract

Introduction

Conclusions

References

Tables

Figures

◀

▶

◀

▶

Back

Close

Full Screen / Esc

Printer-friendly Version

Interactive Discussion



The optical depth of each layer is varied.

Figure 3 shows a false colour image of the simulated multi-layer cloud for different layer thickness. The false colour image is created using the 0.67, 0.87 and 1.6 μm channels. Ice crystals are absorbing in the 1.6 μm channel, resulting in the pale blue colour which increases in intensity as the overlapping cloud increases in thickness. Thick liquid clouds also absorb strongly in the 1.6 μm channel.

Figure 4 shows the results of performing non-linear retrievals of single and multi-layer cloud assuming a single layer cloud model and selecting the best retrieval based on the retrieval, liquid or ice, with the lowest cost. The plots show the retrieved value of the cloud parameter and the corresponding cost, or goodness of fit. Figure 5 shows the percentage differences between the “true” and retrieved cloud parameters. These retrieved values are then contrasted with the retrieval error for the cloud parameter, the following points are noted.

- All retrievals converged regardless of if the retrieval was accurate or not.
- Multi-layered clouds where the upper ice layer had an optical depth of ≤ 1 generally fit the liquid LUTs best. In these cases the retrieved properties were closer to the true liquid cloud.
- The most poorly retrieved cases were thin ice clouds over thick liquid cloud. In these cases the effective radius of the ice cloud was underestimated, the clouds placed too low in the atmosphere and the retrieved optical depth underestimated. These scenarios did not always exhibit the highest retrieval error, however the cost is nearly always greater than 1 in these cases.
- The ice cloud parameters are retrieved with higher accuracy and low cost when the lower layer of liquid cloud is very thin compared to the upper layer.
- The cloud phase selected on the basis of cost is generally liquid when the ice layer is thin (i.e. less than 1–3 optical depths) relative to the lower cloud layer.

Cloud retrieval algorithm

C. A. Poulsen et al.

Title Page

Abstract

Introduction

Conclusions

References

Tables

Figures

◀

▶

◀

▶

Back

Close

Full Screen / Esc

Printer-friendly Version

Interactive Discussion



retrieval errors will nearly always reflect the error on the retrieval. However the authors realise that these results are simulations and in real cases other sources of high cost may obscure a little the multi-layer detection.

Liquid and ice water path are derived from the retrieved optical depth and effective radius. For lack of other information the cloud is assumed to be a single phase, ice or liquid in the calculation of retrieved IWP/LWP. For reference the “true” LWP/IWP is calculated for each layer using the correct phase by applying Eq. (17). In general the retrieval of IWP and LWP has a smaller percentage error than the optical depth and effective radius individually as the optical depth and effective radius tend to compensate for each other to achieve a more accurate IWP of LWP. When the cloud is very thick, i.e. optical; depth > 50, then the IWP/LWP are underestimated. For scenes with thick ice cloud over water cloud the IWP/LWP are often overestimated. In difficult (i.e. retrievals with high cost) multi-layer scenarios the retrieved cloud ice/liquid water path is underestimated. The global bias caused by this will depend on the type and frequency of multi-layered clouds.

12 Example retrieval

In this section we show an example retrieval of cloud using ATSR-2 data from 10 November 1999 over Europe. Figure 6 shows the false colour image and the cost of the retrieval. The pale blue colouring denotes the likely presence of ice cloud due to absorption in the 1.6 μm channel. The scene comprises a variety of cloud types over land and sea. Directly over Switzerland is some thick ice cloud, towards the Italian coast the cloud is thin liquid cloud. The value of the cost is high where the cloud is thin or the scene is clear. Elevated costs are also apparent over thicker cloud banks, perhaps indicating the presence of multi-layered cloud. The white spaces within the ATSR swath images show where no cloud has been detected using the cloud mask (see Sect. 7 for details on cloud mask used).

Cloud retrieval algorithm

C. A. Poulsen et al.

Title Page

Abstract

Introduction

Conclusions

References

Tables

Figures

◀

▶

◀

▶

Back

Close

Full Screen / Esc

Printer-friendly Version

Interactive Discussion



Figures 7 to 10 show the retrieved cloud parameters, the associated error in the retrieval and the selected cloud phase. From these figures the following observations are made.

- Cloud top pressure appears to be realistic. The error on the cloud top pressure retrieval is highest where the cloud is thin and the surface contribution to the TOA radiances becomes significant.
- The uncertainty in the optical depth retrievals is proportional to the thickness of the cloud, i.e. thick clouds have the highest error in optical depth.
- Ice clouds are retrieved with a higher effective radius than liquid clouds. The uncertainty is highest when the clouds are thin.
- Low cloud fractions are typically retrieved at the edges of larger cloud fields.
- The cost is highest when the cloud is thin or where there is no cloud visible to the eye in the false colour image. Enhanced cost values are visible around the edge of identified cloud fields, possibly due to 3-D radiative transfer effects such as shadowing.
- Ice cloud phase is collocated with clouds identified as being high or with large effective radii, as would be expected.
- There is a clear discontinuity in the cost as it goes from sea to land due to the albedo-related error assignment described in Sect. 10.1. More well tuned assignment of surface forward model would reduce the land/sea discontinuity.

The retrievals from the ATSR-2 scene over Europe appear consistent with the simulated retrievals described previously. A more complete validation of the cloud properties can be found in Sayer et al. (2010).

Cloud retrieval algorithm

C. A. Poulsen et al.

Title Page

Abstract

Introduction

Conclusions

References

Tables

Figures

◀

▶

◀

▶

Back

Close

Full Screen / Esc

Printer-friendly Version

Interactive Discussion



13 A dataset of cloud properties from ATSR

The algorithm has been applied to ATSR data to produce the GRAPE dataset of cloud parameters from July 1995 to June 2003 (from ATSR-2), and has being processed from August 2002–2009 (from AATSR). There was a 6 month data outage from January to June 1996 caused by a temporary scan mirror failure. The cloud parameters provided are outlined in Table 2. Further details, data, documentation, quality statements and imagery of products can be found at the British Atmospheric Data Centre (BADC) website, www.badc.ac.uk.

14 Conclusions

A method of optimally retrieving cloud parameters from passive visible through infrared satellite data has been described. The algorithm is capable of using the instrument noise characteristics and a priori information with associated retrieval errors to provide cloud macro and microphysical properties (cloud optical depth, effective radius, cloud top pressure and cloud fraction). The algorithm is based around a forward model which uses look up tables for computational speed. The LUTs for liquid cloud droplets are based on Mie scattering while the ice LUTs are calculated using optical properties from ice crystals. A key advantage of this technique is that it uses all channels, and derives all parameters, simultaneously, meaning the resulting cloud parameters are radiatively consistent with the measurements. In addition the retrieval provides two quality control measures: the cost and the expected errors. The cost assesses the quality of fit to the model used and where the fit is good then the accuracy of the retrieval is based on the expected error. By basing the selection of phase on the lowest cost retrieval correct cloud phase could be deduced in most cloud scenarios.

Using linear simulations the retrieval is found to be accurate for single layer clouds except when the cloud is very thin < 1 optical depths or approaching very high optical depths i.e. typically > 50 . Non-linear retrieval simulations have been performed to

Cloud retrieval algorithm

C. A. Poulsen et al.

Title Page

Abstract

Introduction

Conclusions

References

Tables

Figures

◀

▶

◀

▶

Back

Close

Full Screen / Esc

Printer-friendly Version

Interactive Discussion



Cloud retrieval algorithm

C. A. Poulsen et al.

Title Page

Abstract

Introduction

Conclusions

References

Tables

Figures

◀

▶

◀

▶

Back

Close

Full Screen / Esc

Printer-friendly Version

Interactive Discussion



5 assess the sensitivity of the retrievals to assuming a single layer cloud and to the choice of incorrect phase used to retrieve cloud properties. For many multi-layer cloud scenarios, i.e. when the layers are of comparable thickness or the lower layer is thin and the upper layer is greater than five optical depths, the retrieval is relatively robust. However retrievals of multi-layer cloud when the upper ice cloud layer is very thin, i.e. less than five optical depths will generally retrieve cloud top pressure and cloud effective radius which are an average of the two-layers. The retrievals of optical depth are relatively robust but are underestimated when the two-layer cloud is very thick.

10 In addition to the state parameters retrieved directly by the algorithm, cloud liquid or ice water path are derived. These are underestimated in multi-layer situations, except when the lower layer is very thick compared to the upper layer. As thin ice cloud over water cloud scenario is relatively frequent, users of the data should consider the cost and retrieval error when using the data. The cost and retrieval errors have been identified as useful quality indicators to assess when the model used is appropriate and retrieval is accurate.

15 The technique has been demonstrated using satellite data from ATSR-2. The ATSR-2/AATSR data set can be downloaded at www.badc.co.uk. The algorithm is applicable to most passive visible, near infrared and infrared sensors such as ATSR, MODIS, AVHRR and SEVIRI.

20 *Acknowledgements.* The authors would like to thank EUMETSAT for funding the original algorithm development. This work was supported by the Natural Environment Research Council (grant numbers NERC/T/S/2001/002 and NERC/C513393/1). The authors would also like to thank ESA and the NEODC for providing the ATSR data, ECMWF for providing ECMWF ERA-40 data and NASA for the MODIS albedo dataset.

References

- Austin, R. T, and Stephens, G. L.: Retrieval of stratus cloud microphysical parameters using millimeter-wave radar and visible optical depth in preparation for CloudSat, 1. Algorithm formulation, *J. Geophys. Res.*, 106, 28233–28242, 2001.
- 5 Baran, A. J. and Havemann, S.: The dependence of retrieved cirrus ice-crystal effective dimension on assumed ice-crystal geometry and size-distribution function at solar wavelengths, *Q. J. Roy. Meteorol. Soc.*, 130, 2153–2167, doi:10.1256/qj.03.154, 2004. 2397
- Baran, A. J., Shcherbakov, V. N., Baker, B. A., Gayet, J. F., and Lawson, R. P.: On the scattering phase function of non-symmetric ice crystals, *Q. J. Roy. Meteorol. Soc.*, 131, 2609–2616, 10 2005. 2403
- Berk, A., Bernstien, L. S., and Robertson, D. C.: MODTRAN A moderate resolution model for LOWTRAN7, Airforce Geophysics Laboratory, Hanscom AFB, MA, GL-TR-89-0122, 38 pp., 1989.
- 15 Birks, A.: Improvements to the AATSR IPF relating to land surface temperature, ESA Technical note, AATSR Product Handbook, Issue 1.2, European Space Agency, Esrin Frascati, Italy, 2004. 2404
- Bodas-Salcedo, A., Webb, M. J., Brooks, M. E., Ringer, M. A., Williams, K. D., Milton, S. F., and Wilson, D. R.: Evaluating cloud systems in the Met Office global forecast model using simulated CloudSat radar reactivities, *J. Geophys. Res.*, 113, D00A13, 20 doi:10.1029/2007JD009620, 2008. 2392
- Bulgin, C. E., Palmer, P. I., Thomas, G. E., Arnold, C. P. G., Campmany, E., Carboni, E., Grainger, R. G., Poulsen, C., Siddans, R., and Lawrence, B. N.: Regional and seasonal variations of the Twomey indirect effect as observed by the ATSR-2 satellite instrument, *Geophys. Res. Lett.*, 35, L02811, doi:10.1029/2007GL031394, 2008. 2393
- 25 Campmany, E., Grainger, R. G., Dean, S. M., and Sayer, A. M.: Automatic detection of ship tracks in ATSR-2 satellite imagery, *Atmos. Chem. Phys.*, 9, 1899–1905, doi:10.5194/acp-9-1899-2009, 2009. 2393
- 30 Chang, F.-L., Li, Z., and Clothiaux, E. E.: Comparing the Overlapped Cloud Top Altitudes Deduced from A Satellite-Based Retrieval Scheme with Atmospheric Radiation Measurement Ground-Based Measurement, Fifteenth ARM Science Team Meeting Proceedings, Daytona Beach, Florida, 14–18 March, 2005. 2408

AMTD

4, 2389–2431, 2011

Cloud retrieval algorithm

C. A. Poulsen et al.

Title Page

Abstract

Introduction

Conclusions

References

Tables

Figures

◀

▶

◀

▶

Back

Close

Full Screen / Esc

Printer-friendly Version

Interactive Discussion



Cloud retrieval algorithm

C. A. Poulsen et al.

Title Page

Abstract

Introduction

Conclusions

References

Tables

Figures

◀

▶

◀

▶

Back

Close

Full Screen / Esc

Printer-friendly Version

Interactive Discussion



- Cox, C. and Munk, W.: Measurement of the roughness of the sea surface from photographs on the Sun's glitter, *J. Opt. Soc. Am.*, 44, 838–850, doi:10.1364/JOSA.44.000838, 1954. 2396
- Cox, C. and Munk, W.: Statistics of the sea surface derived from Sun glitter, *J. Mar. Res.*, 13, 198–227, 1954. 2396
- 5 Delanoe, J. and Hogan, R. J.: A variational scheme for retrieving ice cloud properties from combined radar, lidar and infrared radiometer, *J. Geophys. Res.*, 113, D07204, doi:10.1029/2007JD009000, 2008.
- ECMWF: ERA-40 archive web page, <http://www.ecmwf.int/research/era/Products/> (last access: 10 April 2011), 2008. 2396
- 10 Evan, A. T., Heidinger, A. K., Vimont, D. J.: Arguments against a physical long-term trend in global ISCCP cloud amounts, *Geophys. Res. Lett.*, 34, L04701, doi:10.1029/2006GL028083, 2007. 2392
- GEWEX web page, <http://www.gewex.org>, last access: 10 April, 2011.
- Ham, S.-H., Sohn, B.-J., Yang, P., and Baum, B.: Assessment of the quality of MODIS Cloud products from radiance simulations, *J. Appl. Meteorol.*, 48, 1591–1612, 2009. 2392
- 15 Han, Q., Rossow, W. B., and Lasis, A. A.: Near-Global Survey of Effective Droplet Radii in Liquid Water Clouds Using ISCCP Data, *J. Climate*, 7, 465–497, 1994. 2405
- Heidinger, A. K. and Pavlonis, M. J.: Gazing at cirrus clouds for 25 years through a split window, Part I: methodology, *J. Appl. Meteorol.*, 48, 1110–1116, doi:10.1175/2008JAMC1882.1, 2009. 2391
- 20 Intergovernmental Panel on Climate Change: Climate Change 2007 The Physical Science Basis, Contribution of working group 1 to the Fourth Assessment Report of the Intergovernmental Panel on Climate Change, edited by: Solomon, S., Qin, D., Manning, M., Chen, Z., Marquis, M., Averyt, K. B., Tignor, M., and Miller, H., Cambridge Univ Press, Cambridge, UK, 2007.
- 25 Jacobowitz, H., Stowe, L. L., Ohring, G., Heidinger, A., Knapp, K., and Nalli, N. R.: The Advanced Very High Resolution Radiometer Pathfinder Atmosphere (PATMOS) climate dataset: A resource for climate research, *B. Am. Meteorol. Soc.*, 84(6), 785–793, 2003. 2391
- Levenberg, K.: A method for the solution of certain nonlinear problems in least squares, *Quart. Appl. Math.*, 2, 164–168, 1944. 2395
- 30 Liou, K. N.: An introduction to atmospheric radiation, Academic Press, New York, 1980.

**Cloud retrieval
algorithm**

C. A. Poulsen et al.

Title Page

Abstract

Introduction

Conclusions

References

Tables

Figures

◀

▶

◀

▶

Back

Close

Full Screen / Esc

Printer-friendly Version

Interactive Discussion



- Llewellyn-Jones, D., Edwards, M. C., Mutlow, C. T., Birks, A. R., Barton, L. J., and Tait, H., AATSR:Global-change and surface-temperature measurements from Envisat, *ESA Bull.*, 105, 10–21, 2001. 2393
- Marquardt, D. W.: An algorithm for least-squares estimation of nonlinear parameters, *SIAM, J. Appl. Math.*, 11, 431–441, doi:10.1137/0111030, 1963. 2395
- Merchant, C. J., Harris, A. R., Maturi, E., and Maccallum, S., Probabilistic physically based cloud-screening of satellite infra-red imagery for operational sea surface temperature retrieval, *Q. J. Roy. Meteorol. Soc.*, 131, 2735–2756, 2005.
- Merchant, C. J., Le Borgne, P., Roquet, H., and Marsouin, A.: Sea surface temperature from a geostationary satellite by optimal estimation, *Remote. Sens. Environ.*, 113(2), 445–457, 2009.
- Mie, G.: Beiträge zur optik trüber medien, speziell kolloidaler metallösungen, *Ann. Phys.*, 330, 377–445, doi:10.1002/andp.19083300302, 1908.
- Moroney, C., Davies, R., and Muller, J.-P.: Operational Retrieval of Cloud-top Heights Using MISR Data, *IEEE T. Geosci. Remote*, 40, 1532–1540, 2002. 2391
- Muller, J.-P., Denis, M.-A., Dundar, R., Mitchell, K. L., Naud, C., and Mannstien, H.: Stereo cloud-top heights and cloud fraction retrieval from ATSR-2, *Int. J. Remote Sens.*, 28, 1921–1938, doi:10.1080/01431160601030975, 2007. 2391
- Mutlow, C. T., Zavody, A. M., Barton, I. J., and Llewellyn-Jones, D. T.: Sea-surface temperature-measurements by the Along-Track Scanning Radiometer on the ERS-1 Satellite – early results, *J. Geophys. Res.-Oceans*, 99(C11), 22575–22588, 1994. 2394
- Mutlow, C. T., Murray, M. J., Bailey, P., Birks, A. R., and Smith, D. L.: ATSR-1/2 user guide issue 1, *ESA User Guide*, 1999. 2393
- Nakajima, T., Tanaka, M., and King, M. D.: Determination of the optical thickness and effective particle radius of clouds from reflected solar radiation measurements, Part I: Theory., *J. Atmos. Sci.*, 47, 187–193, 1990. 2391
- Platnick, S.: Vertical photon transport in cloud remote sensing problems, *J. Geophys. Res.*, 105, 22919–22935, 2000. 2410
- Platnick, S., King, M. D., Ackerman, S. A., Menzel, W. P., Baum, B. A., Riedl, C., and Frey, R. A.: The MODIS cloud products: Algorithms and examples from Terra, *IEEE T. Geosci. Remote, Aqua Special Issue*(41), 459–473, 2003. 2391
- Rodgers, C. D.: Retrieval of atmospheric temperature and composition from remote measurements of thermal radiation, *Rev. Geophys. Space Phys.*, 14(4), 609–624, 1996.

Cloud retrieval algorithm

C. A. Poulsen et al.

Title Page

Abstract

Introduction

Conclusions

References

Tables

Figures

◀

▶

◀

▶

Back

Close

Full Screen / Esc

Printer-friendly Version

Interactive Discussion



- Rodgers, C. D.: Characterization and error analysis of profiles retrieved from remote sounding measurements, *J. Geophys. Res.*, 95, 5587–5595, 1990.
- Rodgers, C. D.: Inverse methods for atmospheric sounding: Theory and Practice/Series on Atmospheric, Oceanic and Planetary Physics, Vol. 2, World Scientific, 2000. 2392, 2395
- 5 Rossow, W. B. and Schiffer, R. A.: ISCCP cloud data products, *B. Am. Meteorol. Soc.*, 72(1), 2–20, 1991. 2391
- Saunders, R. W., Matricardi, M., and Brunel, P.: An Improved Fast Radiative Transfer Model for Assimilation of Satellite Radiance Observations, *Q. J. Roy. Meteorol. Soc.*, 125, 1407–1425, 1999. 2402
- 10 Sayer, A. M. and Grainger, R. G.: Ship tracks: modification of cloud properties and radiative forcing estimate from ATSR-2 data, *Meteorol. Z.*, submitted, 2010. 2393
- Sayer, A. M., Poulsen, C. A., Arnold, C., Campmany, E., Dean, S., Ewen, G. B. L., Grainger, R. G., Lawrence, B. N., Siddans, R., Thomas, G. E., and Watts, P. D.: Global retrieval of ATSR cloud parameters and evaluation (GRAPE): dataset assessment, *Atmos. Chem. Phys. Discuss.*, 10, 25619–25686, doi:10.5194/acpd-10-25619-2010, 2010. 2390, 2412
- 15 Schaaf, C. B., Gao, F., Strahler, A. H., Lucht, W., Li, X., Tsang, T., Strugnell, N. C., Zhang, X., Jin, Y., Muller, J.-P., Lewis, P., Barnsley, M., Hobson, P., Disney, M., Roberts, G., Dunderdale, M., Doll, C., d'Entremont, R., Hu, B., Liang, S., Privette, J. L., and Roy, D. P.: First Operational BRDF, Albedo and Nadir Reflectance Products from MODIS, *Remote Sens. Environ.*, 83, 135–148, 2002.
- 20 Schaepman-Strub, G., Schaepman, M. E., Painter, T. H., Dangel, S., Martonchik, J. V.: Reflectance quantities in optical remote sensing- definitions and case studies, *Remote Sens. Environ.*, 103, 27–42, 2006. 2400
- Siddans, R., Poulsen, C., and Carboni, E.: Cloud Model for operational retrievals from MSG-SEVIRI, Eumetsat Final report: contract EUM/CO/07/4600000463/PDW, 2009. 2392
- 25 Smith, D.: Report for ATSR VisMon contract, ESA Technical note, 2005. 2403
- Smith, D., Poulsen, C., and Latter, B.: Calibration status of the AATSR reflectance channels, 2008 ESA MERIS/(A)ATSR Workshop, 2008. 2394
- Smith, D. L., Delderfield, J., Drummond, D., Edwards, T., Mutlow, C. T., Read, P. D., and Toplis, G. M.: Calibration of the AATSR Instrument, *Adv. Space Res.*, 28(1), 31–39, 2001. 2394
- 30 Smith, D. L., Mutlow, C. T., and Rao, C. R. N.: Calibration monitoring of the visible and near-infrared channels of the Along-Track Scanning Radiometer-2 by use of stable terrestrial sites, *Appl. Optics*, 41, 515–523, doi:10.1364/AO.41.000515, 2002.

Cloud retrieval algorithm

C. A. Poulsen et al.

Title Page

Abstract

Introduction

Conclusions

References

Tables

Figures

◀

▶

◀

▶

Back

Close

Full Screen / Esc

Printer-friendly Version

Interactive Discussion



- Stamnes, K., Tsay, S. C., Wiscombe, W., and Jayaweera, K.: Numerically stable algorithm for discrete ordinate method radiative transfer in multiple scattering and emitting layered media, *Appl. Optics*, 12, 2502–2509, 1988. 2398
- Stephens, G. L., Vane, D. G., Tanelli, S., Im, E., Durden, S., Rokey, M., Reinke, D., Partain, P., Mace, G. G., Austin, R., Ecuyer, T., Jaynes, J., Lebsock, N., Suzuki, K., Walisder, D., Wu, D., Kay, J., Gettelman, A., Wang, Z., and Marchand, R.: CloudSat mission: Performance and early science after the first year of operation, *J. Geophys. Res.*, 113, D00A18, doi:10.1029/2008JD009982, 2008. 2391
- Takano, Y. and Liou, K. N.: Solar radiative transfer in cirrus clouds, Part I: Single-scattering and optical properties of hexagonal ice crystals, *J. Atmos. Sci.*, 46, 3–19, 1989. 2397
- Thomas, G. E., Poulsen, C. A., Sayer, A. M., Marsh, S. H., Dean, S. M., Carboni, E., Siddans, R., Grainger, R. G., and Lawrence, B. N.: The GRAPE aerosol retrieval algorithm, *Atmos. Meas. Tech.*, 2, 679–701, doi:10.5194/amt-2-679-2009, 2009. 2393
- Watts, P. D., Mutlow, C. T., Baran, A. J., and Zavody, A. M.: Study on cloud properties derived from Meteosat Second Generation Observations, *Eumetsat Report*, http://www.eumetsat.int/idcplg?IdcService=GET_FILE&dDocName=PDF_SCI_97181_MSG-CLOUD-PROPS&RevisionSelectionMethod=LatestReleased (last access: 10 April 2011), 1998. 2393, 2403
- Winker, D. M., Hunt, W. H., and McGill, M. J.: Initial performance assessment of CALIOP, *Geophys. Res. Lett.*, 34, L19803, doi:10.1029/2007GL030135, 2007. 2391
- Wylie, D. P. and Menzel, W. P.: Eight years of high cloud Statistics using HIRS, *J. Climate*, 12, 170–184, 1999. 2391
- Zavody, A. M., Mutlow, C. T., and Llewellyn-Jones, D. T.: Cloud clearing over the ocean in the processing of data from the along-track scanning radiometer (ATSR), *J. Atmos. Ocean. Tech.*, 17, 595–615, 2000. 2404
- Zhang, Z., Yang, P., Kattawar, G., Riedi, J., Labonnote, L. C., Baum, B. A., Platnick, S., and Huang, H.-L.: Influence of ice particle model on satellite ice cloud retrieval: lessons learned from MODIS and POLDER cloud product comparison, *Atmos. Chem. Phys.*, 9, 7115–7129, doi:10.5194/acp-9-7115-2009, 2009. 2408

Cloud retrieval algorithm

C. A. Poulsen et al.

Title Page

Abstract

Introduction

Conclusions

References

Tables

Figures

◀

▶

◀

▶

Back

Close

Full Screen / Esc

Printer-friendly Version

Interactive Discussion



Table 2. ATSR retrieved cloud properties units and range.

Parameter	Units	range
Cloud optical depth	\log_{10}	0–320
Cloud effective radius	μm	0–120
Cloud top pressure	hPa	1000–100
Cloud fraction		0–1
Cloud phase	liquid/ice	0/1

Cloud retrieval algorithm

C. A. Poulsen et al.

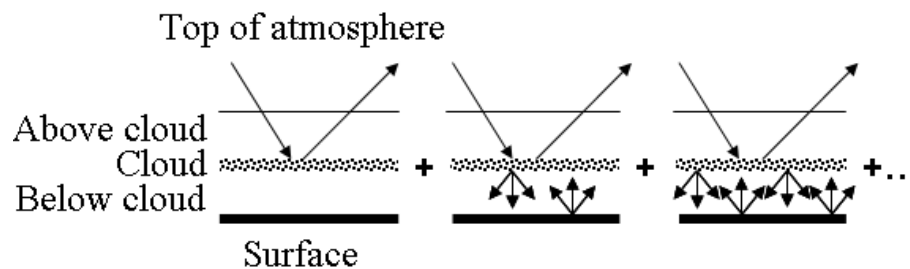


Fig. 1. Schematic of the contributions to the measured radiance through multiple scattering between the atmosphere and surface.

Title Page

Abstract

Introduction

Conclusions

References

Tables

Figures

◀

▶

◀

▶

Back

Close

Full Screen / Esc

Printer-friendly Version

Interactive Discussion



Cloud retrieval algorithm

C. A. Poulsen et al.

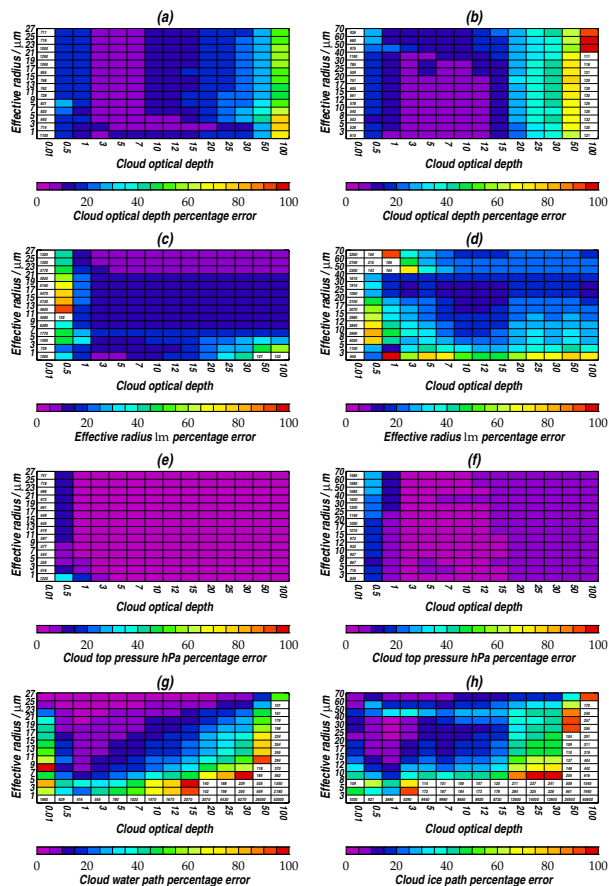


Fig. 2. Simulated retrieval error as a function of varying effective radii and cloud optical depth for cloud optical depth (a) and (b), effective radius (c) and (d), cloud top pressure (e) and (f) and cloud liquid/ice path (g) and (h). Results for simulated liquid (left) and simulated ice (right) single layer cloud over sea.

Title Page

Abstract

Introduction

Conclusions

References

Tables

Figures

◀

▶

◀

▶

Back

Close

Full Screen / Esc

Printer-friendly Version

Interactive Discussion



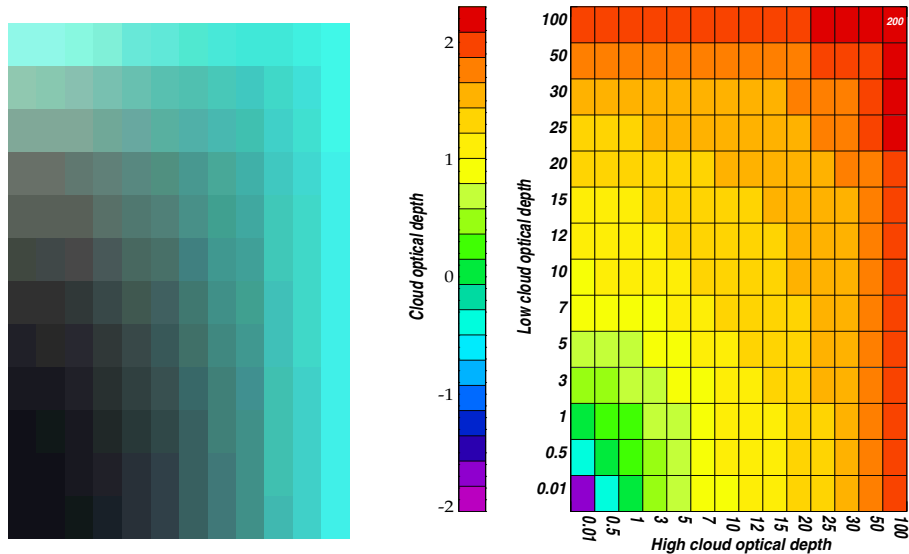


Fig. 3. False colour image of the simulated multi-layered cloud cases (left) and the simulated total optical depth (right). The optical depths simulated were, 0.01, 0.1, 0.3, 1., 2., 3., 5., 7.5, 10., 20, 30, 100 for each layer.

Cloud retrieval algorithm

C. A. Poulsen et al.

Title Page

Abstract Introduction

Conclusions References

Tables Figures

◀ ▶

◀ ▶

Back Close

Full Screen / Esc

Printer-friendly Version

Interactive Discussion



Cloud retrieval algorithm

C. A. Poulsen et al.

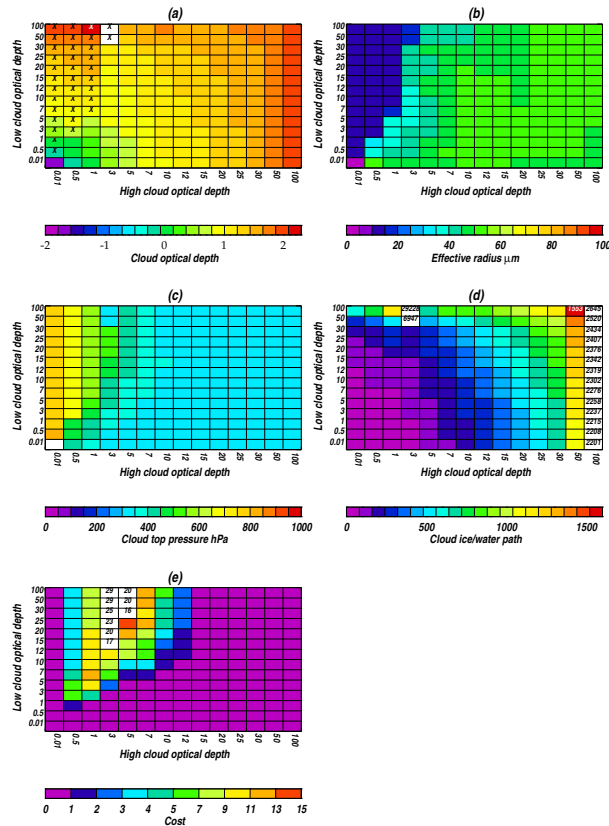


Fig. 4. Non-linear retrievals of single and multi-layer cloud performed using a single layer cloud model using the LUT (cloud or ice) that produced the lowest cost. Plots (a), (b), (c), (d) show the retrieved optical depth, effective radius and cloud top pressure and cloud liquid/ice path, respectively. The phase of the best retrieval is indicated on plot (a) the “X” indicates the best retrieval was a liquid cloud. Plot (e) shows the cost.

Title Page

Abstract Introduction

Conclusions References

Tables Figures

◀ ▶

◀ ▶

Back Close

Full Screen / Esc

Printer-friendly Version

Interactive Discussion



Cloud retrieval algorithm

C. A. Poulsen et al.

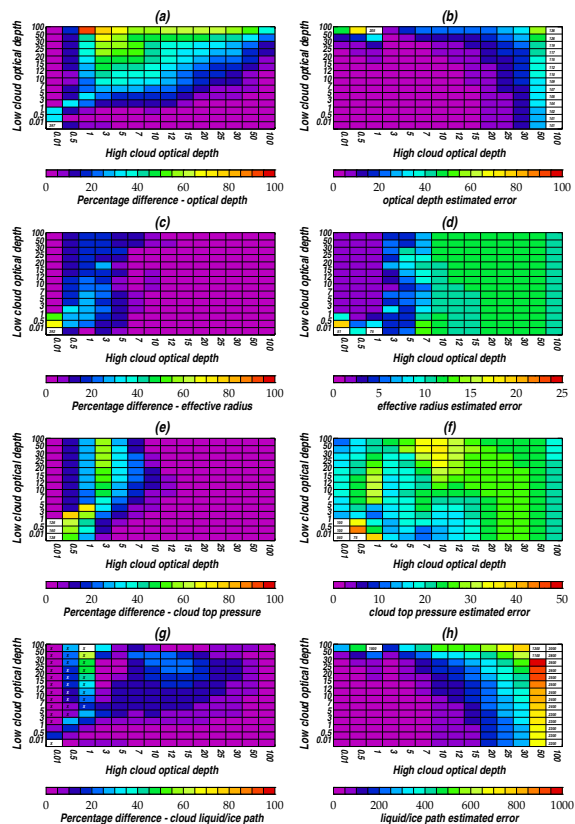


Fig. 5. Plots showing the percentage differences between the “true” and retrieved cloud parameter, left column, compared to the retrieval error for the cloud parameter, right column. From top to bottom the results are shown for optical depth, effective radius, cloud top pressure and cloud liquid/ice path. The “truth” is defined by the phase selected. The “X” in plot (g) denotes when a water phase was selected as the retrieval with the lowest cost as per Fig. 4.

Title Page

Abstract

Introduction

Conclusions

References

Tables

Figures

◀

▶

◀

▶

Back

Close

Full Screen / Esc

Printer-friendly Version

Interactive Discussion



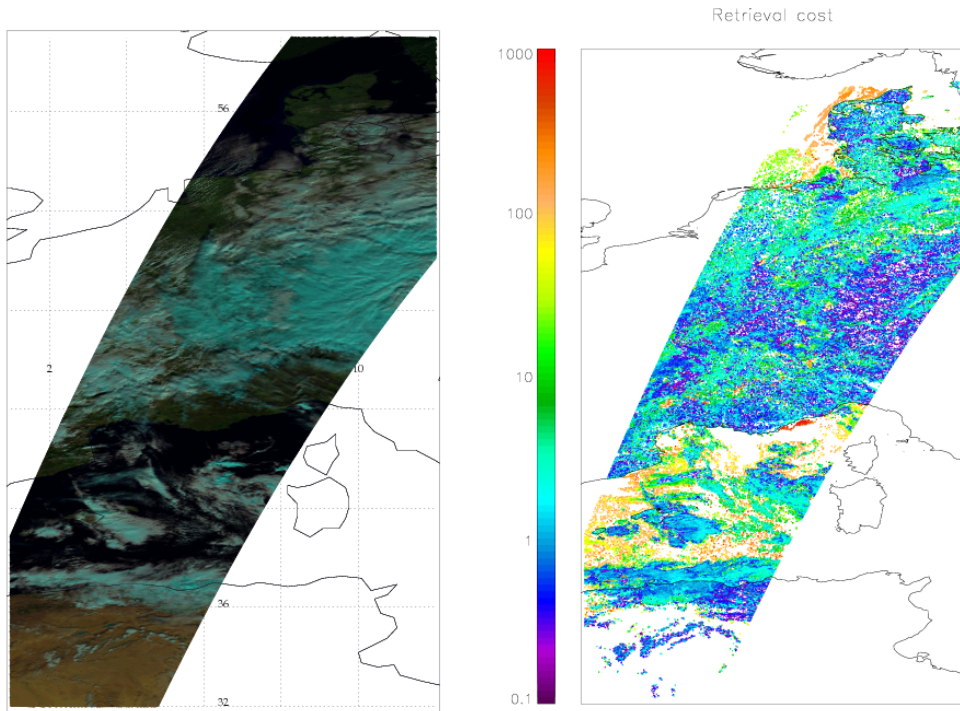


Fig. 6. False colour image of clouds over Europe. The pale blue colour results from absorption in the $1.6 \mu\text{m}$ channel and is an indicator of ice phase or very thick clouds (left) and cost of the retrieval.

Cloud retrieval algorithm

C. A. Poulsen et al.

Title Page

Abstract Introduction

Conclusions References

Tables Figures

◀ ▶

◀ ▶

Back Close

Full Screen / Esc

Printer-friendly Version

Interactive Discussion



Cloud retrieval algorithm

C. A. Poulsen et al.

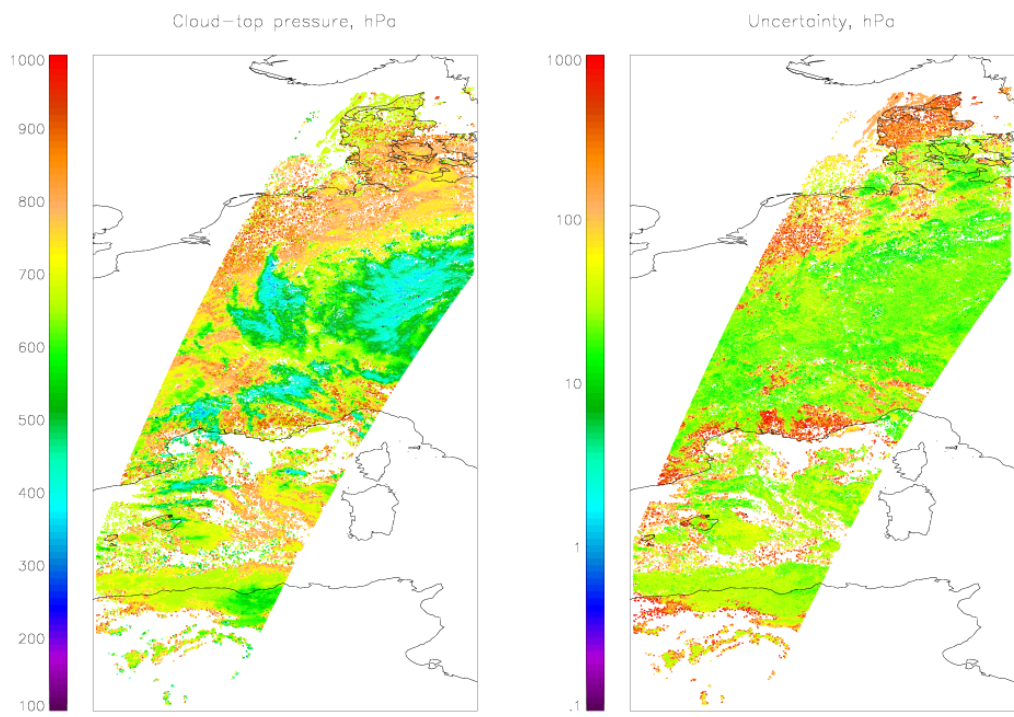


Fig. 7. Cloud top pressure and error on cloud top pressure for the image of Fig. 6.

Title Page

Abstract Introduction

Conclusions References

Tables Figures

◀ ▶

◀ ▶

Back Close

Full Screen / Esc

Printer-friendly Version

Interactive Discussion



Cloud retrieval algorithm

C. A. Poulsen et al.

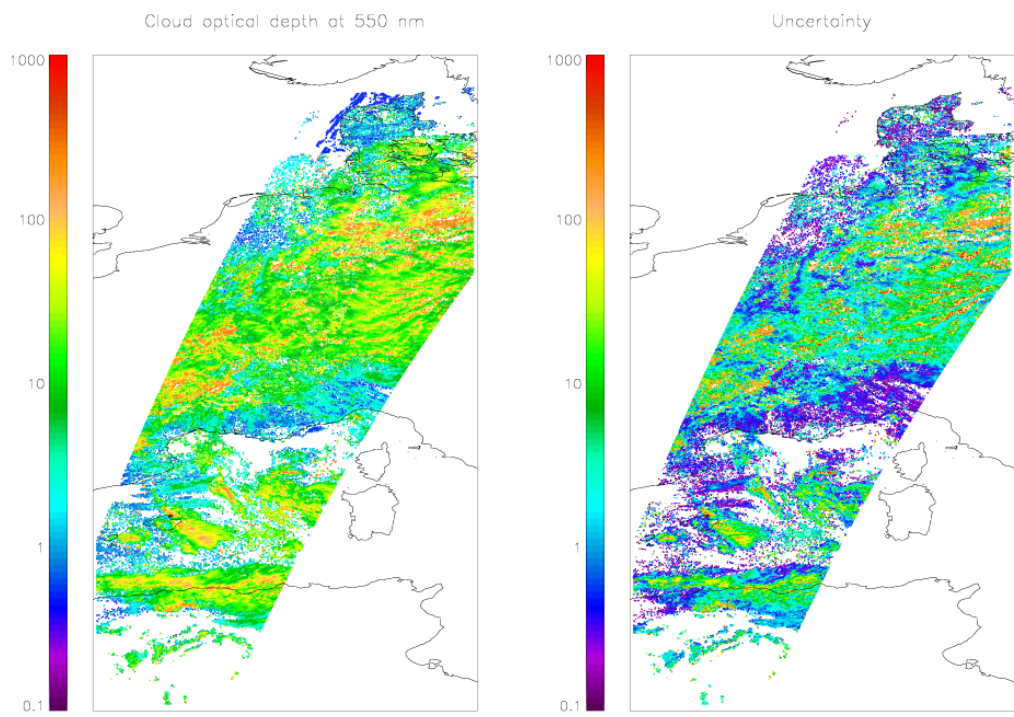


Fig. 8. Cloud optical depth and error on cloud optical depth for the image of Fig. 6.

Title Page	
Abstract	Introduction
Conclusions	References
Tables	Figures
◀	▶
◀	▶
Back	Close
Full Screen / Esc	
Printer-friendly Version	
Interactive Discussion	



**Cloud retrieval
algorithm**

C. A. Poulsen et al.

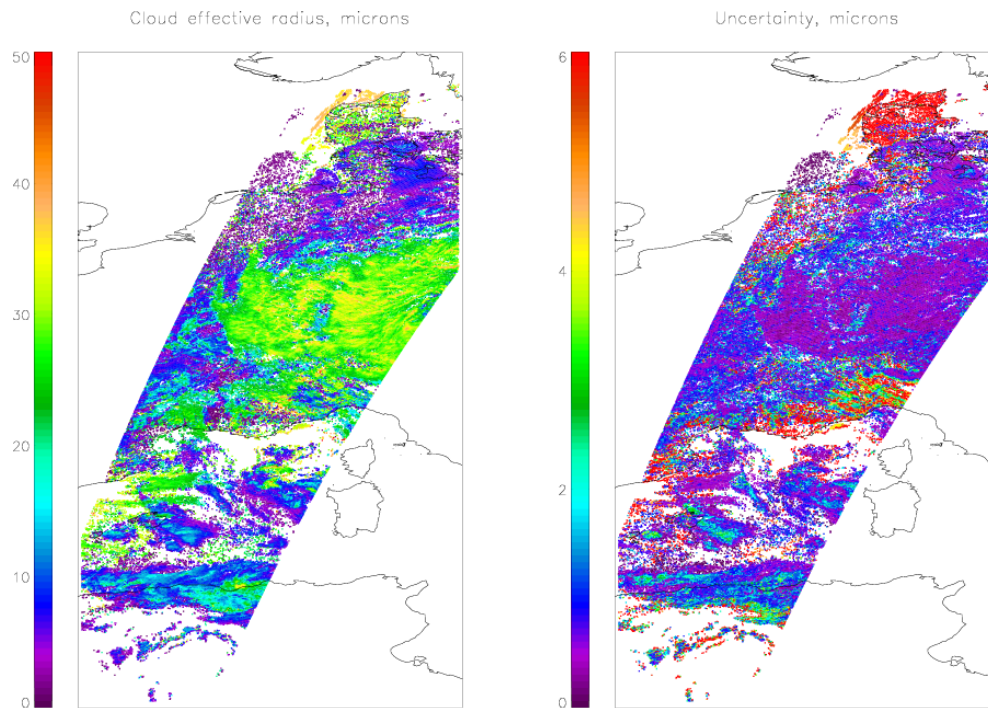


Fig. 9. Cloud effective radius and error on cloud effective radius for the image of Fig. 6.

[Title Page](#)[Abstract](#)[Introduction](#)[Conclusions](#)[References](#)[Tables](#)[Figures](#)[◀](#)[▶](#)[◀](#)[▶](#)[Back](#)[Close](#)[Full Screen / Esc](#)[Printer-friendly Version](#)[Interactive Discussion](#)

Cloud retrieval algorithm

C. A. Poulsen et al.

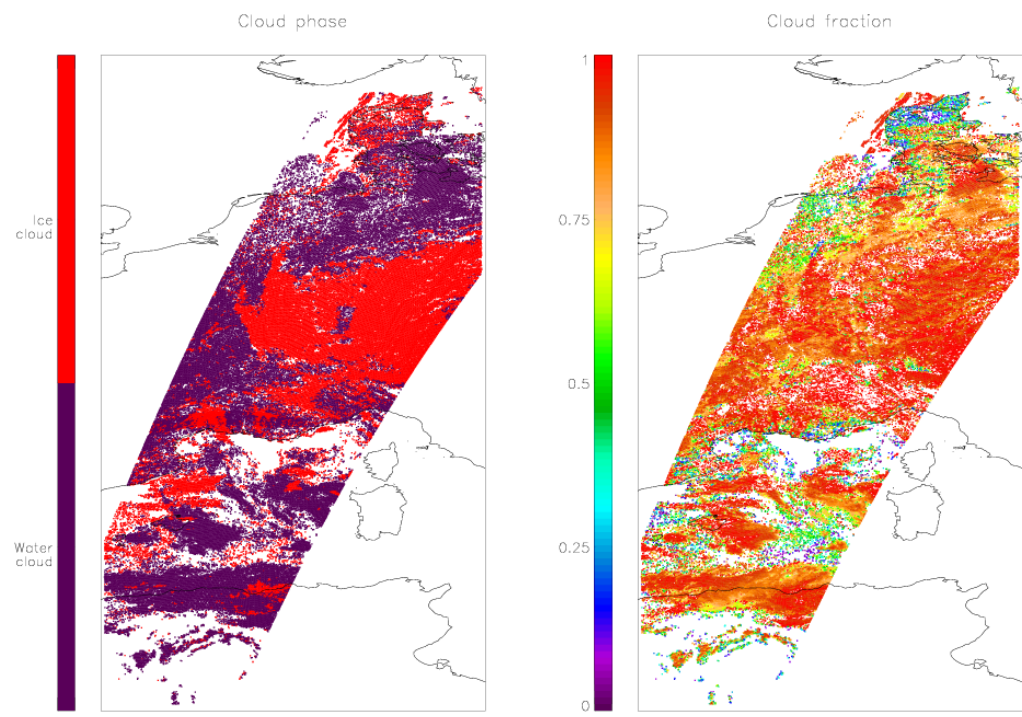


Fig. 10. Cloud phase and Cloud fraction for the image of Fig. 6.

Title Page

Abstract Introduction

Conclusions References

Tables Figures

◀ ▶

◀ ▶

Back Close

Full Screen / Esc

Printer-friendly Version

Interactive Discussion

